Epitaxial growth of CIGSe layers on GaP/Si(001) pseudo-substrate for tandem CIGSe/Si solar cells

Nicolas Barreau, Olivier Durand, Eugène Bertin, Antoine Létoublon, Charles Cornet, Polyxeni Tsoulka, Eric Gautron, Daniel Lincot

Epitaxial growth of CIGSe layers on GaP/Si(001) pseudo-substrate for tandem CIGSe/Si solar cells

Nicolas Barreau[1], Olivier Durand[2], Eugène Bertin[1,2], Antoine Létoublon[2], Charles Cornet[2], Polyxeni Tsoulka[1], Eric Gautron[1], Daniel Lincot[3]

[1] Univ Nantes, CNRS, Institut des Matériaux Jean Rouxel – UMR6502, F-44000 Nantes, France.

[2] Univ Rennes, INSA Rennes, CNRS, Institut FOTON - UMR 6082, F-35000 Rennes, France.

[3] CNRS, Institut Photovoltaïque d'Île de France, Ecole polytechnique-Institut polytechnique de Paris, Chimie Paristech-PSL, UMR 9006, 18 Boulevard Thomas Gobert, 91120 Palaiseau France

Abstract

In this study, the epitaxial growth of co-evaporated Cu(In,Ga)Se_2 films (CIGSe) onto GaP/Si(001) pseudo-substrates, where the GaP thin layer is epitaxially grown by Molecular Beam Epitaxy (MBE), is investigated. Extensive structural characterisation of epi-CIGSe is carried out via X-ray diffraction as well as transmission electron microscopy. Sturdy evidence of an epitaxial growth of CIGSe on (GaP/Si)(001) is observed, with the propagation of twins originating from the GaP/Si interface, through the CIGSe/GaP interface. This work aims at paving the way for future CIGSe/GaP/Si structures for the development of tandem solar cells with a c-Si bottom cell, and a GaP interfacial buffer layer for band edge engineering, allowing for the monolithic epitaxial growth of high quality CIGSe as a thin film top cell absorber.

Keywords

Molecular beam epitaxy, epitaxial CIGSe, gallium phosphide, silicon, XRD structural characterization, TEM

1. Introduction and objectives

In the course of increasing solar cell efficiency beyond the Shockley-Queisser limit being about 33% for a single junction, multijunction architectures and in particular double junction (tandem) ones are the most relevant avenue. The maximum theoretical efficiency of tandem junctions is indeed around 43% [1], explaining the impressive research effort worldwide for accelerating the development of this technology, with the aim of providing PV modules with an efficiency of up to 30% on the market by 2030 [2,3]. The most attractive option is to build onto the existing silicon technology, which will provide a bottom cell, while adding a top cell from existing thin film technology. Today, the mainstream approach is to use perovskite-based device as top cell since this latter provides impressive single junction efficiency up to 25.5% [4]. The silicon–perovskite tandem approach is already developed at the pilot stage level, with champion cell performance of 29.52%, achieved by Oxford-PV [5]. The second option is to use III-V semiconductor devices as top cell, this approach allowed to achieve a 23.7% efficiency [6]. However, these two options suffer from drawbacks, such as the lack of maturity for the perovskite-based (stability, upscaling) approach and wafer bonding technological complexity for the III-V approach [6]. Monolithic integration of III-V semiconductors onto silicon substrate may overcome the latter issue [7]. While being optimistic that the scientific community will soon solve these difficulties, there exists an alternative approach, not considered so far though presenting several advantages with respect to those mentioned before. This option

consists in considering the $Cu(In,Ga)(Se,S)_2$ (CIGS) thin film technology, which is commercially implemented and already achieved record efficiency of 23.35 % [8]. The strategic objective of the present article is to benefit from the already existing infrastructures and create a strong industrial synergy by combining c-Si and CIGS technologies. However, in order to act as a top cell integrated on silicon, the band gap of the CIGS should ideally be close to 1.7 eV [9] and yield conversion efficiency of about 18-20 % [2]. On the one hand, fulfilling the band gap objective is manageable from several combinations, namely either $CuGaSe_2$ (Eg ~ 1.7 eV), $CuIn_{0.7}Ga_{0.3}S_2$ (Eg ~ 1.7 eV) or $Cu(In,Ga)(Se,S)_2$ mixed chalcogenides. On the other hand, the efficiencies reached by cells based on those so-called wide band gap CIGS absorbers are still too low for achieving high performance tandem devices; champion efficiency does not exceed 12 % for $CuGaSe_2$, and is fairly higher for pure sulfides (16.9 % for 1.55 eV [10]). One should notice that these results were obtained for CIGS absorbers deposited onto Mo rear contact, which is not optimal in terms of electronic transport. Shifting to silicon substrates can solve two Mo-related drawbacks. Firstly, the growth onto Mo leads to polycrystalline films, whose grain boundaries are detrimental for such wide band gap CIGS-based solar cells operation [11,12]. Then, the growth onto c-Si may solve this problem if epitaxial growth of CIGS is achieved, thereby avoiding photo-generated carrier recombination through grain boundaries. Secondly, CIGS/Mo (Eg > 1.7 eV) interface is strongly recombinant [13]. Such rear side interface can be improved by replacing the Mo by a selective contact, allowing both hole transfer from CIGS and electron repeal via the introduction of an adapted conduction band discontinuity acting as an electronic barrier (concept schemed in Fig.1). However, because silicon band energetic configuration does not satisfy the second criterion, we propose the original approach consisting in the introduction of a suitable III-V buffer layer, also adapted for epitaxy. This role can be played by GaP and further by (Ga,Al)P, quasi-lattice-matched with silicon, as shown in Fig.2 [14]. Epitaxial growth of CIGSe on silicon and III-V compounds has been already reported [15,16] including recent outstanding results for epitaxial cells based on CIGSe/GaAs (Eg=1.15 eV) yielding 20% cell efficiency [17]. Note that in contrast to GaAs, the lattice mismatch of GaP with pure selenides is very large, especially for $CuInSe_2$ and lower but still important for $CuGaSe_2$, making the task addressed hereafter challenging.

In this work, we explore the possibility of growing epitaxial pure selenide CIGSe, with the nominal composition $CuIn_{0.1}Ga_{0.9}Se_2$, onto GaP/silicon pseudo-substrates. High Ga content in CIGSe reduces the lattice mismatch with the GaP and allows bandgap widening, necessary for tandem applications. The kinetics of pure-Ga CGSe being unfavorable to structural and morphological reorganization [12], adding a little amount of indium is herein motivated by the possible CIGSe restructuration and spontaneous lattice matching with GaP, at the expense of slightly lower lattice matching. An in depth analysis of the epitaxial and structural relationships is carried out, showing that high quality epitaxy of CIGSe can be achieved on GaP/Si.

2. Experimental details

2.1 Epitaxial growth of GaP on Si(001) substrates

First, epitaxial quasi-lattice matched GaP have been grown on Si(001) substrate by Molecular Beam Epitaxy (MBE), to realize III-V/Si pseudo-substrates [18]. 90 nm thin GaP layers have been grown using a RIBER solid-source MBE reactor, on a Si substrate with a 4° miscut towards [110] in order to promote burying of AntiPhase Domains [19,20]. GaP is quasi-lattice-matched to Si, with only a 0.4% mismatch at room temperature. The GaP/Si samples have been grown at 580 °C using a two-step procedure with a first 20 nm- thin MEE (Molecular Enhanced Epitaxy) GaP layer, followed by a 70 nm thin MBE GaP layer (see ref [18] and [21] for more details on the growth process). MEE consists in alternated growth of Ga and P atomic layers, with, in this case, Ga as a prelayer. This technique

allows a pseudo-2D growth mode even at relatively low growth temperature [18,22]. Strategies (Si surface preparation, and growth temperature variations) to mitigate specifically the appearance of micro-twins (MTs) were not used in this work, thus leading to the presence of MTs in the studied samples, contrarily to other state-of-the art GaP/Si samples [21,23]. Indeed, the purpose of this study was to verify the potentiality of the CIGSe growth onto a GaP/Si(001) pseudo-substrate, prior to any thorough growth development.

2.2 $CuIn_{0.1}Ga_{0.9}Se_2$ growth

The investigated nominal $CuIn_{0.1}Ga_{0.9}Se_2$ films were deposited by thermal co-evaporation from elemental sources of Cu (99.999%), Ga (99.9999%), In (99.999%) and Se (99.999%) in a dedicated high vacuum chamber, where the base pressure was below 6.10^{-7} mbar, and did not exceed 3.10^{-6} mbar during deposition. Such a system offers many free parameters such as evaporation fluxes of each element and substrates temperature. During the whole process, the substrates, heated with IR-lamps, were maintained at a temperature of 600°C measured with a thermocouple positioned at the backside of the substrates.

These 1.7 µm-thick CIGSe layers were deposited onto GaP/c-Si(001) platforms previously glued with melted indium onto Mo/soda lime glass (SLG) substrate. This latter procedure ensures that the temperature of GaP/c-Si is homogeneous and similar to that of standardly used Mo/SLG, for which the growth chamber's parameters are optimized. The platforms were cleaned in ultrasonic bath of acetone, then ethanol at room temperature before being dried with N_2.

The process herein implemented is a sequential process called CuPRO, meaning Cu-poor/Rich/Off, initially developed at Uppsala University [24]. Fundamentally, it consists in 3 sequential steps, but differs from the well-known "3-stage" process [25] in that the substrate temperature (600°C) and the In and Ga atomic fluxes (i.e. Φ_{In} and Φ_{Ga}) are kept constant. This less technologically demanding process was chosen because it is compatible with large scale implementation (e.g. constant substrate temperature, lower temperature growth and faster than the regular bithermal 3-stage process [26,27]). During the CuPRO process, the only varying parameter is the Cu atomic flux (Φ_{Cu}), which is set to a value corresponding to $\Phi_{Cu}/(\Phi_{In}+\Phi_{Ga}) \sim 0.8$ during the 1st stage, then increased up to $\Phi_{Cu}/(\Phi_{In}+\Phi_{Ga}) \sim 1.1$ during the 2nd stage, until the growing layer turns Cu-rich. Finally, Cu flux is turned off until the growing layer turns Cu-poor again. The Cu-poor/Cu-rich and Cu-rich/Cu-poor transitions are followed *in situ* thanks to the evolution of the IR-lamps power supplied to maintain the substrates at 600°C (see Fig.3). The targeted global composition of the films corresponds to GGI = [Ga]/([In]+[Ga]) ~ 0.9 and CGI = [Cu]/([In]+[Ga]) ~ 0.95 (*i.e.* slightly Cu-poor). Adding a little amount of indium is herein motivated by possible CIGSe spontaneous lattice matching relative to GaP while the recrystallization occurs during the Cu-rich second step [28,29]. Note that during the whole growth process, excess selenium flux ($10 < \Phi_{Se}/\Phi_{metals} < 20$) is supplied to prevent the formation of detrimental intermetallic phase clusters. The herein applied sequential deposition process is depicted in Fig.3.

2.3 Advanced X-Ray diffraction

X-ray diffraction (XRD) was performed on a 4 circles Bruker D8 diffractometer (horizontal scattering plane geometry) using two different modes of this instrument: (*i*) the standard low-resolution mode used for the pole figures measurements and (*ii*) a high-resolution mode for the $\omega/2\theta$ longitudinal scan mode. This diffractometer is equipped with a 1D Gobel Multi-layer Mirror placed on the linear focus window of a standard sealed tube as primary optics. The feeding power is set to 40 kV/40 mA. The detector is a LynxEye™, 1 dimensional position sensitive detector (PSD). It is used either in PSD

or point detector modes. This PSD is positioned at 300 mm from the goniometer center and presents 180 channels making a maximum of 13.5 mm (2.6°) in the horizontal direction. Details of the XRD experiments can be found in ref [23]. Considering the $\omega/2\theta$ longitudinal scans, particular attention has been paid to the sample adjustments to account for the 4° substrate miscut, aligning the diffraction vector direction with respect to the diffraction planes instead of the sample surface.

2.4 Advanced local characterization by Transmission Electron Microscopy (TEM)

Scanning Transmission Electron Microscopy (S/TEM) characterization was performed on a Cs-probe corrected Themis Z G3 (Thermo Fisher Scientific) operating at 300 kV accelerating voltage. High Angle Annular Dark Field (HAADF) images were acquired with a 21.4 mrad convergence angle and 63-200 mrad collection angles and Energy Dispersive X-ray Spectroscopy (EDS) maps with 4 windowless silicon drift detectors (Super-X system). Four-dimensional STEM (4D-STEM) was implemented to image the 2D electron diffraction pattern on a OneView CMOS camera at each position in a 2D array rastered by the probe. In order to avoid superimposition of the diffracted disks, convergence angle was lowered to 0.65 mrad. TEM cross sectional specimens were prepared by mechanical polishing followed by ion milling (Gatan PIPS 691) at low voltage and low temperature (- 40 °C) to limit sample degradation.

3 Results and discussion

3.1. Epitaxial relationship between the CIGSe and the GaP/Si(001) pseudo-substrate.

Advanced XRD investigations

In the following, we present characteristic features of the structural properties of wide band gap CIGSe films grown on GaP/Si(001) pseudo-substrates, obtained by XRD, for CIGSe layers displaying a global GGI of 0.85 as measured by TEM-EDS, close to the nominal GGI of 0.9. In the tetragonal chalcopyrite system, the lattice parameter c in very close to 2a. Thus, it may prove difficult to discriminate the (00l) from the (h00) broad Bragg reflections. In practice, domains with c axis in the three possible directions in real space may appear [17]. In particular, the ω/2θ longitudinal scan displays only the CIGSe(00*l*) or CIGSe(h00) Bragg diffraction peaks, with h and l even, in the vicinity of the GaP/Si (00*l*) ones (Fig. 4). In this diffraction geometry, the diffraction vector direction is maintained along the [00*l*] crystalline direction of the silicon substrate. Thus, the longitudinal scan reveals at least a strong CIGSe [h00] or [00*l*] texture, either from a fiber texture or an epitaxy, as confirmed by the relatively sharp peak in the ω-transverse scan performed around the CIGSe(400)/(008) Bragg peak (Fig.5). We likely witness a broadening of the CIGSe Bragg peaks in the ω/2θ longitudinal as a consequence of the lattice parameter variation along the growth direction; this is likely due to the sequential process applied for CIGSe film growth, giving rise to a variation of the CIGSe composition along the growth direction. However, we identify two peaks at 2θ = 66.2° and 67.3°, with XRD signal in the range 65° to 67.5°. Such an important dispersion of the CIGSe(400)/(008) Bragg peak cannot be explained solely by the presence of a composition gradient along the growth direction, as a variation of ΔGGI=±0.1 would distribute the CIGSe(008)/(400) reflection on a 2θ window of less than 1°. A typical CIGSe layer with GGI of around 0.8 is expected to exhibit a separation of the CIGSe(400)/(008) reflections (i.e. tetragonal splitting) as a result of the tetragonal distortion (*c/a = 1.97*) : the separate CIGSe(400) and the CIGSe(008) reflections would be found at 2θ = 66.2° and 67.3°. This is compatible with the XRD data, as well as the EDS-TEM data, and might suggest that both a and c lattice parameters are detected along the growth direction. We explain this by the possible presence of at least two different variants of the tetragonal CIGSe crystal (i) one with

its c-axis orthogonal to the pseudo-substrate's surface (a-matched), (ii) and one, or two, with their c-axis lying horizontally on the pseudo-substrate's surface (c/2-matched). Theoretical intensities of the CIGSe(400) and CIGSe(008) reflections are roughly equal. Thus, comparing the experimental intensity of the two reflections may indicate that a higher volume of the c/2-matched CIGSe variant is present in the epi-layer. This could be explained by considering CIGSe's lower lattice mismatch in c/2 (~1.5%) compared to the a-axis (~3.2%), with respect to GaP. Finally, one can notice a weak CIGSe (112) Bragg peak at around 27° attributed to the presence of a residual polycrystalline phase.

Moreover, when scanning in an asymmetric ω/2θ mode, in the vicinity of the (202) GaP/Si Bragg reflection, the (220)/(204) CIGSe Bragg reflection is evidenced (Fig.6). Finally, a XRD pole figure performed on the CIGSe(220)/(204) Bragg diffraction peak displays reciprocal lattice point (RLP) positions at around 45° from the pole figure center (Fig.7). CIGSe(220)/(204) reflections are detected along the four <100> azimuths of the pseudo-substrate. Therefore, XRD measurements reveal a high degree of epitaxy for the CIGSe grown on the GaP/Si pseudo-substrate. One can notice that the RLP centers are shifted downward due to the 4° miscut of the substrate towards the [110] direction. One can also notice reflections found at tilt angles χ=20°. The CIGSe/GaP lattice mismatch allows us to select the CIGSe(220)/(204) reflections alone, eliminating the GaP(202) from the pole figure. These additional reflections may correspond to CIGSe(220)/(204) microtwins (MTs), suggesting twin domains exist in the CIGSe. Indeed, in the tetragonal chalcopyrite system, twin boundaries running on the (112) planes may create additional (102) twin planes precisely tilted by 19.5° with respect to the (001) plane. An additional twinning across the same (112) planes reverts the crystal back to its original orientation. Thus, MTs can be described as the succession of two twin boundaries, separated by a few atomic planes, creating a narrow twin domain propagating along the twinning planes. This is analogous to the observation of MTs reflections at χ = 15.9° on cubic GaP(111) pole figures reported in ref. [21].

TEM investigations

In order to explore the local structural properties of the CIGSe/GaP interface and of the individual layers, we conducted analyses by transmission electron microscopy. Selected area electron diffraction (SAED) patterns were acquired along the sample's cross section after orientating the Si wafer along [110]. These results confirm the epitaxial orientation between the CIGSe, GaP and Si layers (Fig.8). A schematic picture of the proposed atom stacking in CIGSe/GaP/Si evidenced in this work is also given in Fig.8.d. CIGSe orientation is maintained over ¾ of the layer. At the top of CIGSe layer, large grains appear. Their SAED patterns can still be explained by a [110] orientation but with few degrees misorientation. Other results displayed in the Supplementary Information (SI Fig.S1) have shown that twinned grains are also present at the top of the CIGSe layer. These results confirm those obtained by XRD. Twin grains close to the surface should contribute to the total volume twin crystal volume alongside MTs, strengthening the associated XRD reflections at χ=20° (Fig.7).

Energy-dispersive X-ray spectroscopy (EDS) profiles depicted in Fig.9 clearly show that contrary to Cu, the In/Ga atomic ratio varies throughout the CIGSe layer. In content increases from the CIGSe/GaP interface up to the middle of the CIGSe and then decreases towards the CIGSe surface. On the other hand, Ga content profile is opposite, keeping the group III elements (In + Ga) total atomic content similar (GGI ~ 0.85) throughout the whole CIGSe layer. The reason for such an evolution can be either the lattice mismatch between GaP and CIGSe crystalline structures (see SI Tab.S1), which is much more favorable between GaP and $CuGaSe_2$ (~ 3 %) than $CuInSe_2$ (~ 6 %), or the CIGSe growth process itself, which is known to favor the so called V-shaped GGI profiles [30,31].

The STEM-HAADF images presented in the Fig.10 does not evidence any amorphous phase at the interface, corroborating the epitaxial growth of the CIGSe on the GaP/Si pseudo-substrate.

3.2. Evaluation of extended crystalline defects in CIGSe/GaP/c-Si structures

As already mentioned, the purpose of this study was to confirm the potentiality of the CIGSe growth onto a GaP/Si(001) pseudo-substrate, prior to any thorough growth development. Therefore, the GaP/Si(001) pseudo-substrates used in this study were not at the state-of-the-art and contained various extended defects such as microtwins originating from the GaP/Si interface and emerging at the GaP surface [23].

Looking thoroughly at the XRD pole figure performed on the (220)/(204) CIGSe Bragg peak (Fig.7), the RLP localized at around 20° from the pole figure center and displaying low intensity are likely due to some MTs reminiscent from the GaP layer [21] as stated earlier in section 3.1. MTs probably propagate across the CIGSe/GaP interface. Indeed, when performing ω/2θ scan at these RLP positions, we find the same (220)/(204) Bragg diffraction peak positions than for the 45° RLP ones due to the main crystalline phase, showing that the MT RLP (at χ = 20°) originate from the same lattice plane family than in the main phase (at χ = 45°) and not from another crystalline plane family.

Moreover, in order to evaluate the morphology of the monolithic epi-structure, SEM observations were performed on samples cross section (Fig.11).

This image firstly shows that CIGSe/GaP interface is compact and free of voids. As far as the 'bulk' of CIGSe layer is concerned, Fig.11 also reveals specific shapes looking like cracks or crevices. At first glance, these extended crystalline defects could correspond to specific grain boundaries, regularly observed in polycrystalline CIGSe layers, which would contradict the conclusions of the advanced XRD and TEM investigations. Interestingly, these latter are all oriented similarly relative to the plane of the substrate, yielding pyramidal top shapes forming angles of about 71° (see SI Fig.S3). In the case of chalcopyrite crystals, 71° is namely the angle between two planes of the {112} family. Secondly, we observe 51° (59° angles) between the right-sided (left-sided) facets of the pyramids and the pseudo-substrate surface. This may correspond to the 55° expected angle between (112) and (001) planes corrected by the ±4° miscut angle, thus favoring the CIGSe{112} microtwin hypothesis. Additionally, further TEM analyses (see Fig.12) clearly reveal that these defects originate from MTs inside the GaP layer which propagate across the CIGSe/GaP interface in the CIGSe layer.

Indeed, the micro-twins, which originate from the GaP growth on Si wafer [21], give rise to additional spots corresponding to twin domains crystallographic fingerprints, as visible in Fig.12.d compared to the monocrystalline ED pattern Fig.12.c. The virtual dark field image Fig.12.f was obtained by measuring the additional spots intensity only and assigning the resulting value to the corresponding pixel. It clearly shows that this defect propagates (as a bright straight line) across the whole GaP layer, from the c-Si to the CIGSe/GaP interface, and extends over few tens nanometers within the CIGSe layer. This was also observed by classical TEM imaging (see SI Fig.S4). This propagating defect is another signature of the epitaxial growth of CIGSe onto GaP/Si(001) pseudo-substrate. In addition, it is worth mentioning that a pyramidal shape is observed at the CIGSe/GaP interface (see Fig.11). Such irregular faceting is typically observed when antiphase domains are not yet buried [19]. Given that growth conditions were not optimized here, with an overall small thickness of GaP (90nm), this result is therefore not surprising [20]. Interestingly, the in-plane rotation of the GaP crystal by 90° in antiphase domains doesn't seem to impact significantly the crystal quality or orientation of the CIGSe, as expected theoretically from the schematic representation of atoms stacking given in Fig.8.

Finally, the high-resolution HAADF-STEM micrograph presented in SI Fig.S5 also evidences that some of the defects are generated at the heterogeneous CIGSe/GaP interface. These defects however do not propagate over long distances in the sample (in SI Fig.S5, the observed stacking fault only propagates over 10 nm), suggesting that even if CIGSe crystalline structure is not perfect, its adaptability allows to suppress some of the defects created at the interface.

From all these observations, we therefore demonstrated that CIGSe materials can be epitaxially integrated on a III-V/Si platform, with a robust epitaxial relationship. Further development of high efficiency CIGSe/III-V/Si tandem devices are therefore conditioned by (i) the necessity to reduce stacking faults and MTs at the III-V/Si interface, which appear to have drastic impact on the CIGSe crystal quality (voids and crevices), (ii) the management of antiphase domains, that does not seem to impact the crystal quality of the CIGSe, but would certainly impact carriers transport in the III-V epilayer.

4. Conclusions

We report on the epitaxial growth of a Cu(In,Ga)Se_2 film on a GaP/Si(001) pseudo-substrate, using a co-evaporation growth process. Thorough structural analyses, through both XRD and TEM measurements, show evidence of a strong epitaxy of the 1.7 µm thick CIGSe layer. This preliminary study opens up many possibilities for bandgap engineering of the CIGS solar cell back contact and selective transparent contacts, as band lineups and bandgaps can be tuned at will using different compositions in GaAlP or GaAlAs ternary alloys. Work on completed cells using ZnO/CdS/epi-CIGS/III-V/p^+-Si is in progress. In the future, the silicon substrate will be replaced by a silicon bottom cell. It is therefore a first step towards the development of high-efficiency CIGS/Si tandem solar cells.

Figures

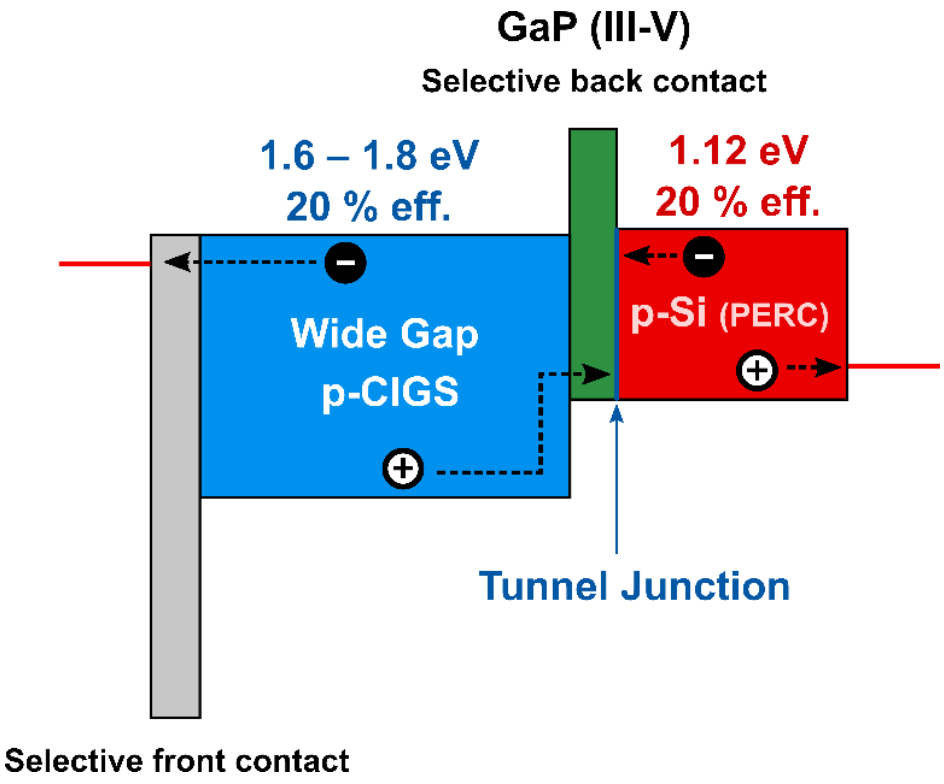

Figure 1: *Energetic diagram for an ideal CIGS/c-Si tandem cell including selective III-V contact at the interface between CIGS and c-Si. Charge carrier pathways are also represented.*

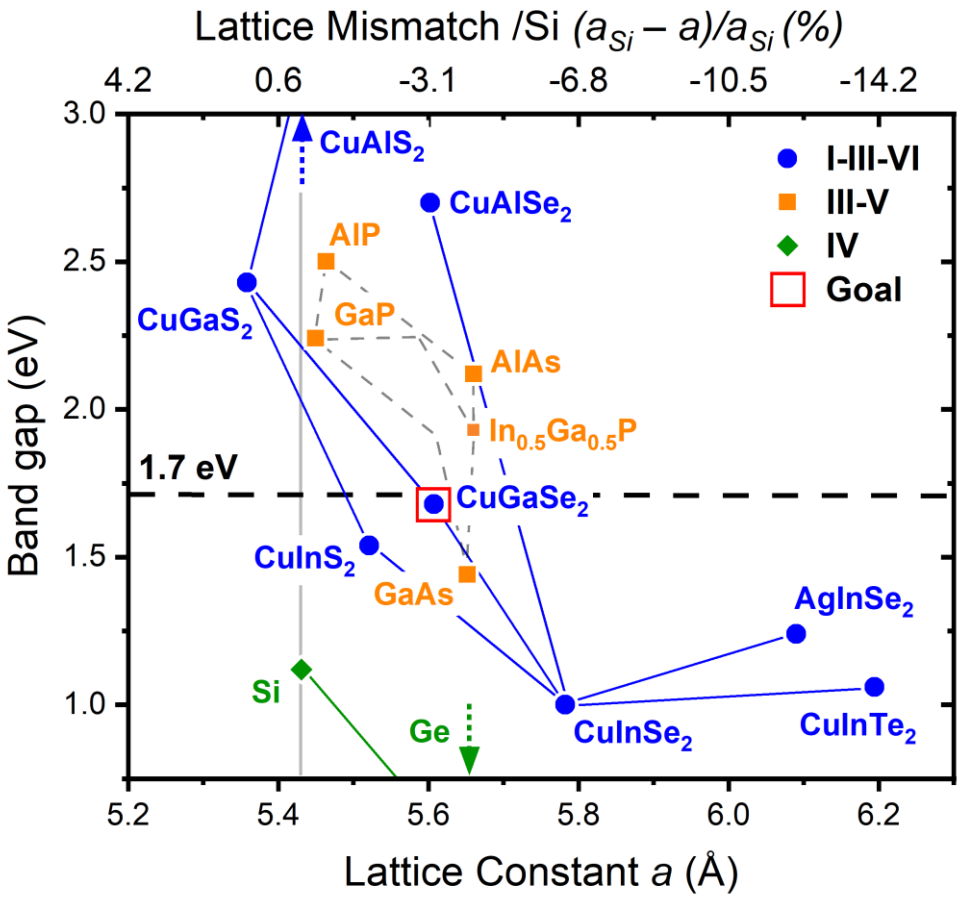

Figure 2: *Band gap vs lattice mismatch for chalcopyrites, silicon and III-V* [14]. *Gallium phosphide GaP is quasi lattice matched with Si. Additionally, in the Cu(In,Ga)(S,Se)$_2$ family, pure-Ga CIGSe selenides have near ideal band gap for top cell applications. Lattice mismatch relative to a_{si} the lattice constant of Si is represented on the top x-axis scale.*

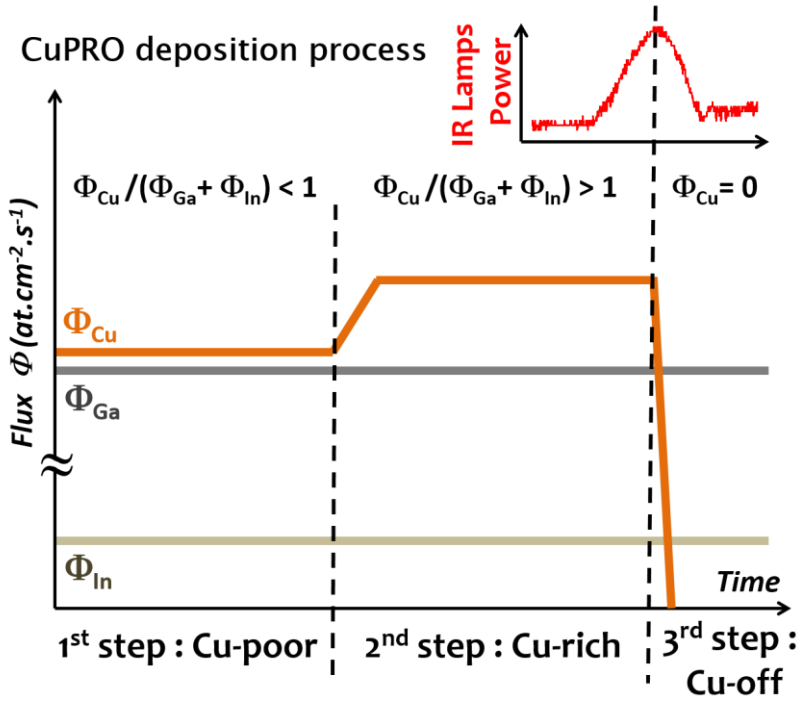

Figure 3: *Evolution of Cu, In and Ga atomic fluxes (Φ) during the whole deposition process. Inset: output power of IR-lamps showing Cu-poor/Cu-rich/Cu-poor transitions.*

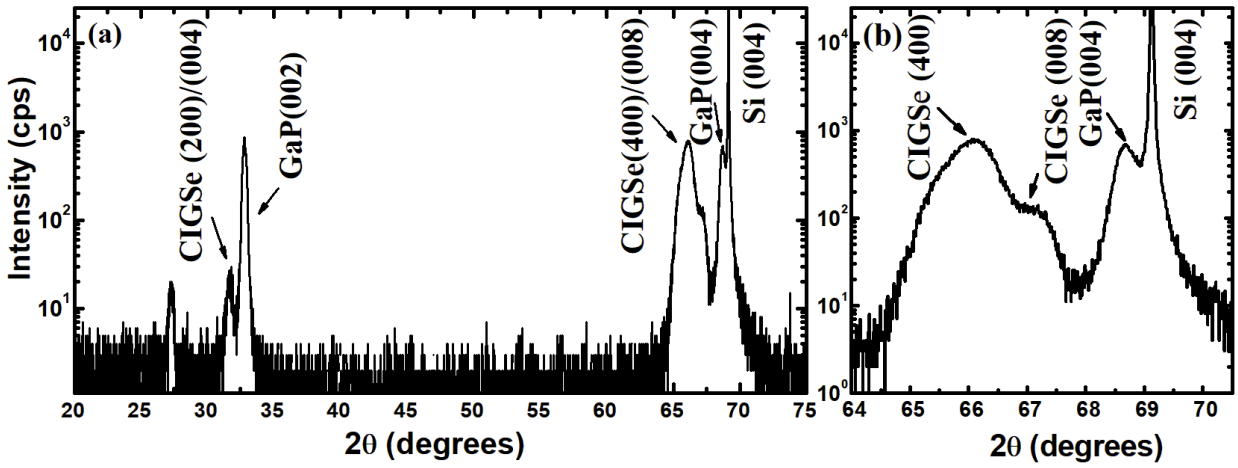

Figure 4: *ω/2θ longitudinal scan on the CIGSe/GaP/Si sample.* ***(a)*** *wide ω/2θ scan displaying intense (00l) and (h00) reflections with even h and l, compatible with the CIGSe chalcopyrite structure* ***(b)*** *Focus around the GaP(004) peak showing evidence of the tetragonal splitting of the CIGSe(400) and CIGSe(008) reflections*

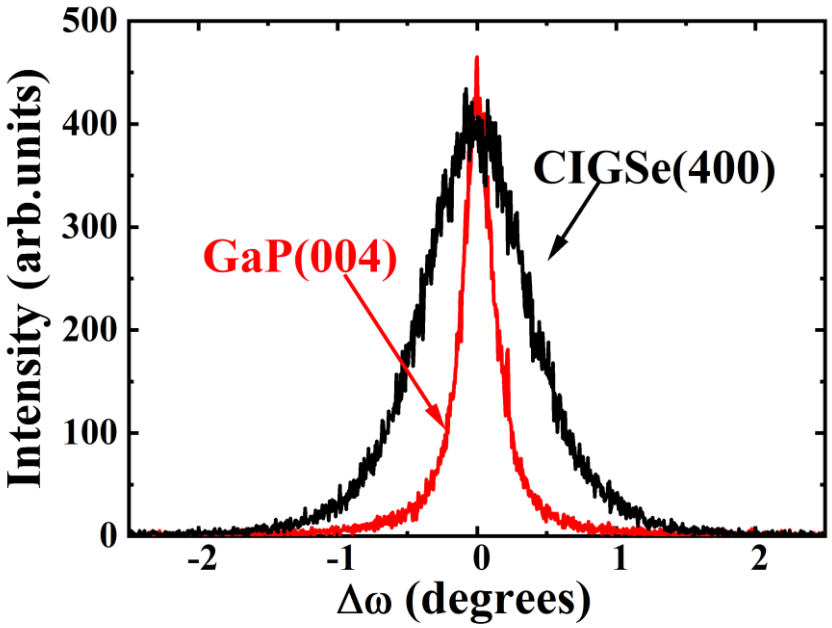

Figure 5: *XRD ω transverse scan selecting the CIGSe(400) reflection (black), as compared to the GaP(004) reflection (red)*

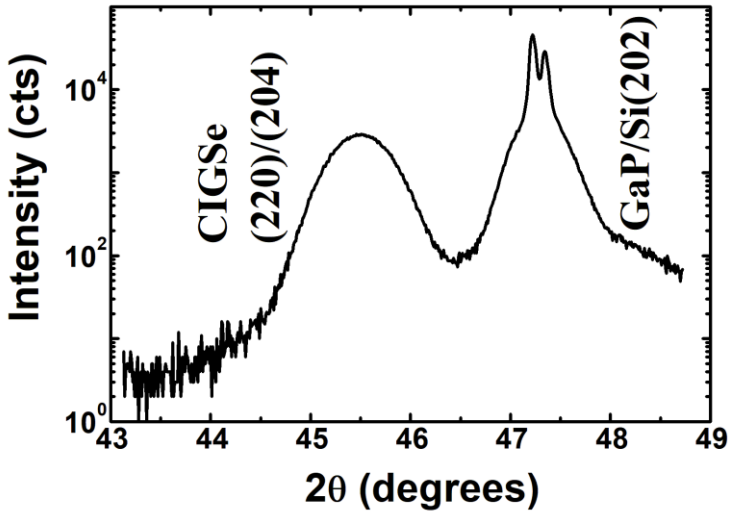

Figure 6: *$\omega/2\theta$ scan around the (202) GaP/Si Bragg reflection (oblique planes) on the CIGSe/GaP/Si sample, showing the (220)/(204) CIGSe Bragg reflection.*

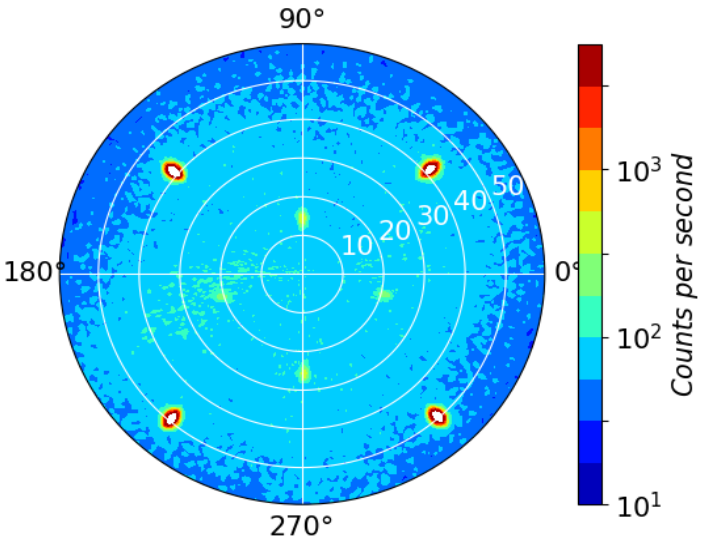

Figure 7: *Pole figure on the CIGSe(220)/(204) Bragg peak. Weaker reflections at χ=20° are attributed to the presence of MTs. The CIGSe/GaP lattice mismatch allows to select the CIGSe(220)/(204) reflections alone, eliminating the GaP(202) from the pole figure.*

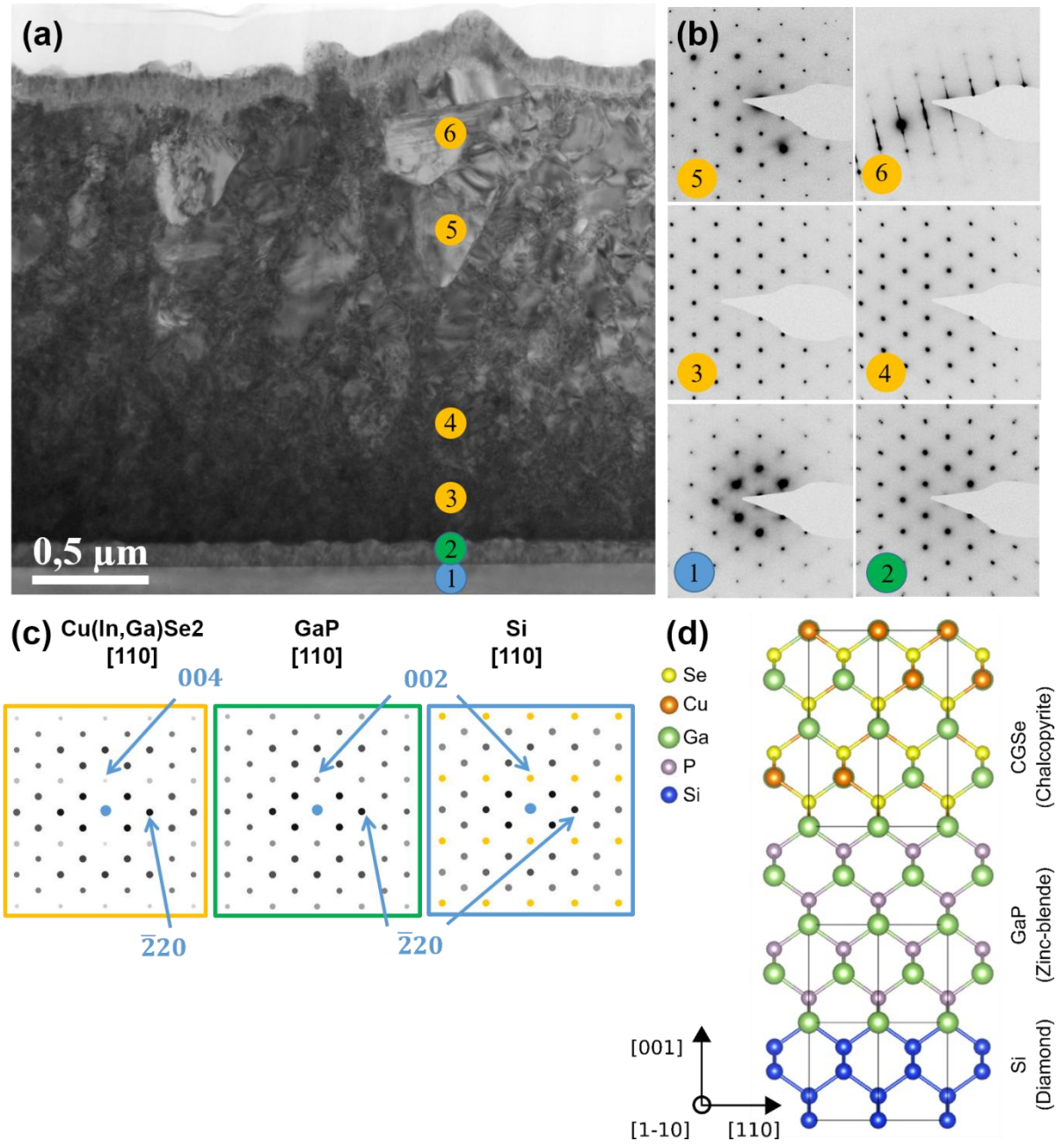

Figure 8: (a) *Cross section TEM bright field micrograph.* ***(b)*** *Selected area electron diffraction patterns acquired in Si substrate (1), GaP layer (2) and CIGSe layer (3 to 6).* ***(c)*** *Simulated electron diffraction patterns of Si, GaP and CIGSe crystalline structures along [110].* ***(d)*** *Corresponding schematic of the crystalline structures stacking considering the CIGSe a-matched crystallographic variant. The figure represents the pure-Ga CGSe chalcopyrite structure for simplicity's sake*

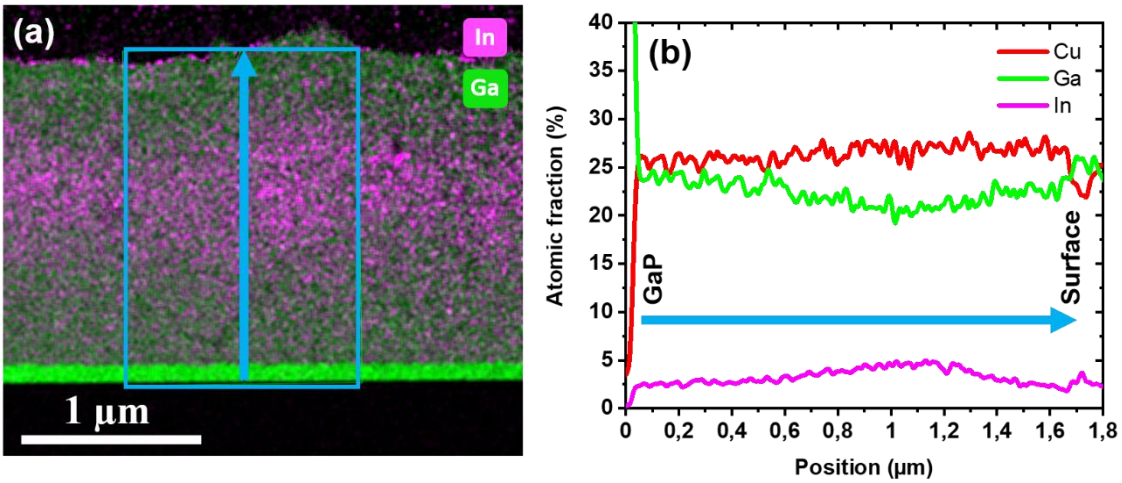

Figure 9: ***(a)*** *Cross section Energy-dispersive X-ray spectroscopy (EDS) mapping (pink: In, green: Ga).* ***(b)*** *Corresponding spectrum profile obtained by integrating the signal in the blue box from the CIGSe/GaP interface to the CIGSe surface (pink: In, green: Ga, red: Cu).*

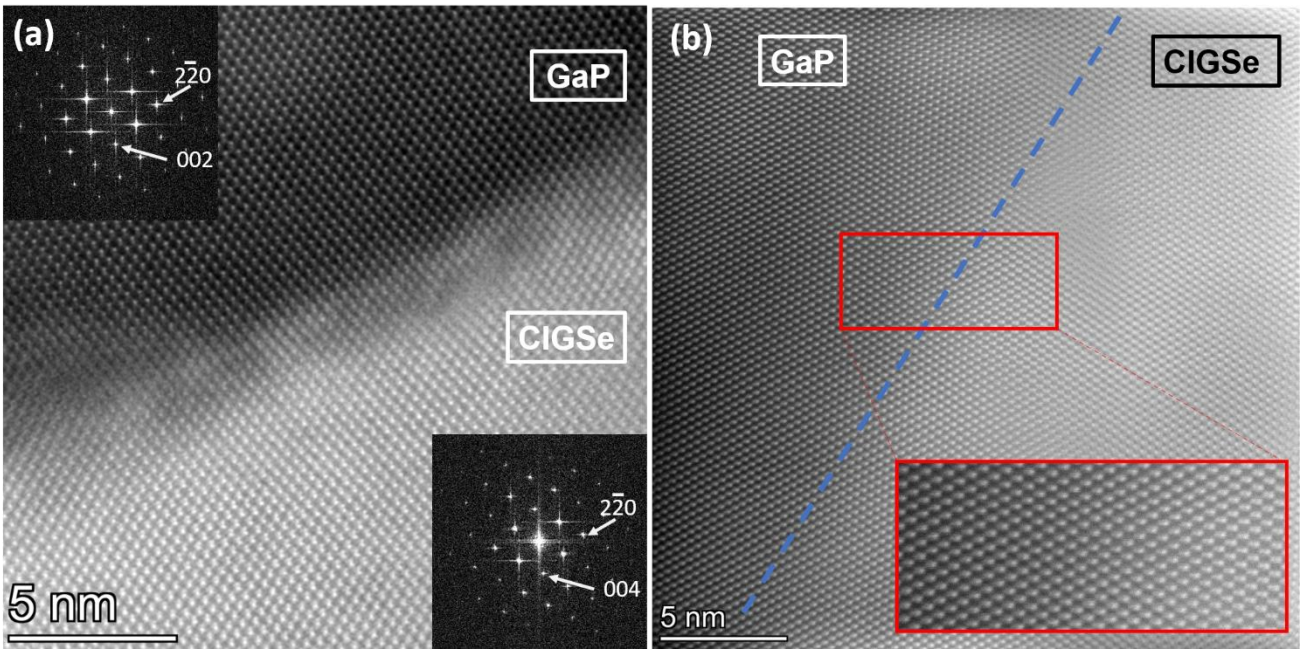

Figure 10: ***(a)*** *STEM-HAADF image of the interface between the CIGSe and the GaP layers in the [110] zone-axis direction (with FFT of each layer as insets), showing the epitaxy between both layers. Fast Fourier transforms are unable to discriminate CIGSe's growth direction.* ***(b)*** *STEM-HAADF image displaying an abrupt and ordered CIGSe/GaP interface after Wien filtering.*

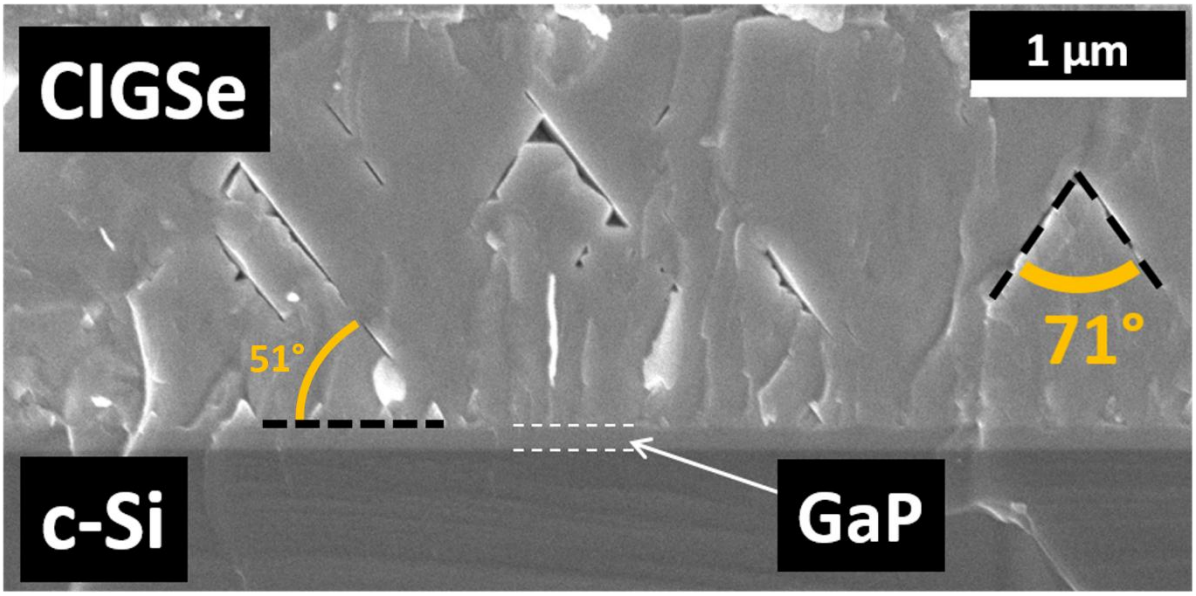

Figure 11: *SEM cross section of the investigated CIGSe/GaP/ c-Si structure*.

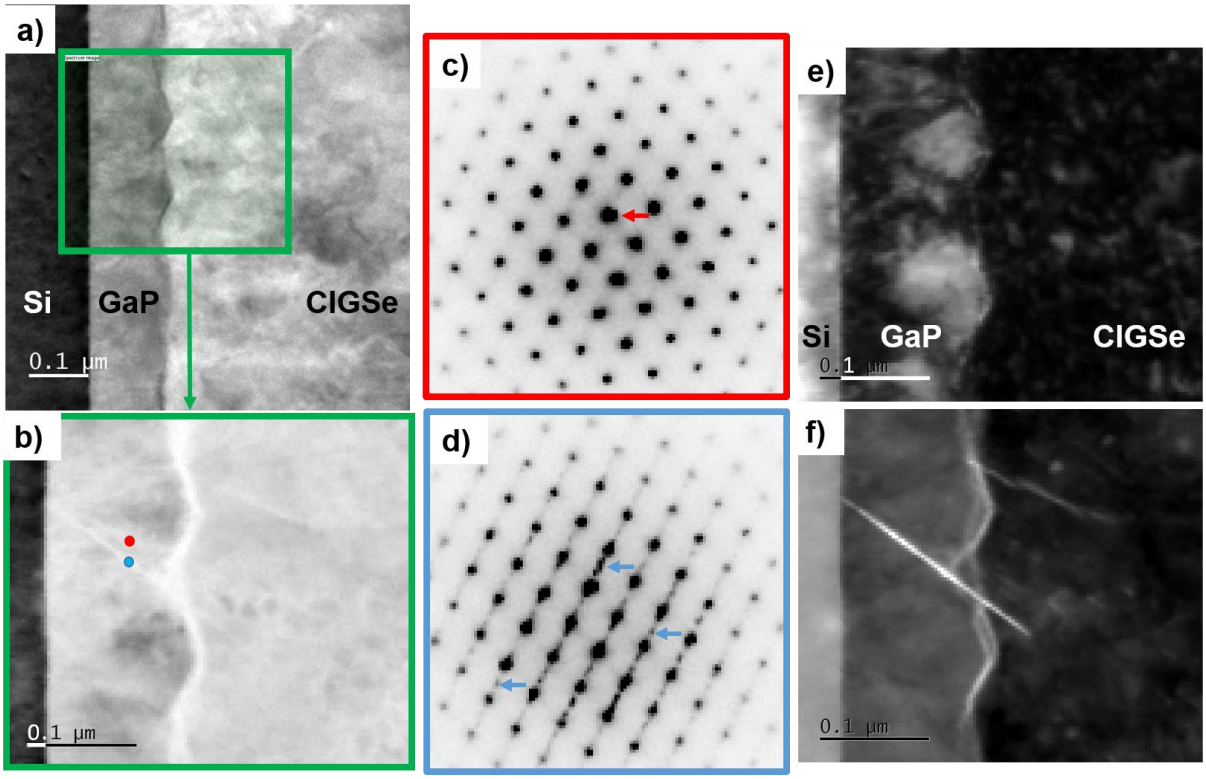

Figure 12: *4D STEM analysis of CIGSe/GaP/c-Si cross section sample.* ***(a)*** *STEM-HAADF image of the stacked layers.* ***(b)*** *4D STEM map in which each pixel contains a 2D electron diffraction (ED) pattern.* ***(c)*** *and* ***(d)*** *Extracted ED patterns at pixels defined by red and blue points in (b). ED pattern in (d) clearly show additional spots compared to (c). Some of these additional diffracted spots are marked by blue arrows.* ***(e)*** *Virtual bright field image obtained by selecting only the transmitted beam (red arrow) in the ED patterns with a numerical mask.* ***(f)*** *Virtual dark field image obtained by selecting only the additional diffracted spots in the ED patterns with a numerical mask.*

Declaration of competing interest

This manuscript is the authors' original work and has not been published or has it been submitted simultaneously elsewhere.

CRediT authorship contribution statement

Nicolas Barreau: Resources, Conceptualization, Methodology, Writing - review & editing. Olivier Durand: Resources, Project administration, Writing - review & editing. Eugène Bertin: Investigation, Writing -review & editing .Antoine Létoublon: Formal analysis, Visualization. Charles Cornet: Resources. Polyxeni Tsoulka: Investigation, Writing - review & editing. Eric Gautron: Investigation, Formal analysis, Writing -review & editing. Daniel Lincot: Conceptualization, Methodology, Validation, Writing -review & editing.

Acknowledgment The authors acknowledge RENATECH+ (French Network of Major Technology Centers) for technological support, the CIMEN Electron Microscopy Center in Nantes and Sciences Chimiques de Rennes for access to the XRD goniometers. This research was supported by the French ANR EPCIS Project (Grant No. ANR-20-CE05-0038), the PIA (Grant no. ANR-IEED-002-01), the French Contrat Plan État-Région and the European Regional Development Fund of Pays de la Loire

References

[1] W. Shockley, H.J. Queisser, Detailed Balance Limit of Efficiency of p-n Junction Solar Cells, Journal of Applied Physics. 32 (1961) 510–519. https://doi.org/10.1063/1.1736034.

[2] T.P. White, N.N. Lal, K.R. Catchpole, Tandem Solar Cells Based on High-Efficiency c-Si Bottom Cells: Top Cell Requirements for >30% Efficiency, IEEE Journal of Photovoltaics. 4 (2014) 208–214. https://doi.org/10.1109/JPHOTOV.2013.2283342.

[3] [30/30/30] initiative for the PV modules • IPVF - L'Institut Photovoltaïque d'Île-de-France, IPVF - L'Institut Photovoltaïque d'Île-de-France. (2015). https://www.ipvf.fr/fr/the-303030-initiative-for-the-modules/ (accessed April 13, 2021).

[4] D. Koo, Y. Cho, U. Kim, G. Jeong, J. Lee, J. Seo, C. Yang, H. Park, High-Performance Inverted Perovskite Solar Cells with Operational Stability via n-Type Small Molecule Additive-Assisted Defect Passivation, Advanced Energy Materials. 10 (2020) 2001920. https://doi.org/10.1002/aenm.202001920.

[5] Oxford PV, Oxford PV hits new world record for solar cell | Oxford Photovoltaics, (n.d.). https://www.oxfordpv.com/news/oxford-pv-hits-new-world-record-solar-cell (accessed April 13, 2021).

[6] E. Veinberg-Vidal, L. Vauche, K. Medjoubi, C. Weick, C. Besançon, P. Garcia-Linares, A. Datas, A. Kaminski-Cachopo, P. Voarino, P. Mur, J. Decobert, C. Dupré, Characterization of dual-junction III-V on Si tandem solar cells with 23.7% efficiency under low concentration, Progress in

Photovoltaics: Research and Applications. 27 (2019) 652–661. https://doi.org/10.1002/pip.3128.
[7] M. Feifel, D. Lackner, J. Schön, J. Ohlmann, J. Benick, G. Siefer, F. Predan, M. Hermle, F. Dimroth, Epitaxial GaInP/GaAs/Si Triple-Junction Solar Cell with 25.9% AM1.5g Efficiency Enabled by Transparent Metamorphic AlxGa1−xAsyP1−y Step-Graded Buffer Structures, Solar RRL. 5 (2021) 2000763. https://doi.org/10.1002/solr.202000763.
[8] M. Nakamura, K. Yamaguchi, Y. Kimoto, Yusuke Yasaki, T. Kato, H. Sugimoto, Cd-Free Cu(In,Ga)(Se,S)2 thin-film solar cell with record efficiency of 23.35%, IEEE Journal of Photovoltaics. 9 (2019) 1863–1867. https://doi.org/10.1109/JPHOTOV.2019.2937218.
[9] S. P. Bremner, M. Y. Levy, C. B. Honsberg, Analysis of tandem solar cell efficiencies under AM1.5G spectrum using a rapid flux calculation method, Progress in Photovoltaics: Research and Applications. 16 (2008) 225–233. https://doi.org/10.1002/pip.799.
[10] H. Sugimoto, H. Hiroi, Y. Iwata, A. Yamada, RECENT PROGRESS IN HIGH EFFICIENCY PURE SULFIDE CIGS SOLAR CELLS, in: 2017.
[11] M. Raghuwanshi, E. Cadel, P. Pareige, S. Duguay, F. Couzinie-Devy, L. Arzel, N. Barreau, Influence of grain boundary modification on limited performance of wide bandgap Cu(In,Ga)Se2 solar cells, Appl. Phys. Lett. 105 (2014) 013902. https://doi.org/10.1063/1.4890001.
[12] P. Tsoulka, A. Rivalland, L. Arzel, N. Barreau, Improved CuGaSe2 absorber properties through a modified co-evaporation process, Thin Solid Films. 709 (2020) 138224. https://doi.org/10.1016/j.tsf.2020.138224.
[13] T. Ott, F. Schönberger, T. Walter, D. Hariskos, O. Kiowski, O. Salomon, R. Schäffler, Verification of phototransistor model for Cu(In,Ga)Se2 solar cells, Thin Solid Films. 582 (2015) 392–396. https://doi.org/10.1016/j.tsf.2014.09.025.
[14] D. Lincot, N. Barreau, A. Ben Slimane, T. Bidaud, S. Collin, M. Feifel, F. Dimroth, M. Balestrieri, D. Coutancier, S. Béchu, M. Bouttemy, A. Etcheberry, O. Durand, M.-A. Pinault-Thaury, F. Jomard, Exploring new convergences between PV technologies for high efficiency tandem solar cells : Wide band gap epitaxial CIGS top cells on silicon bottom cells with III-V intermediate layers, in: 35th European Photovoltaic Solar Energy Conference and Exhibition (EU PVSEC 2018), Bruxelles, Belgium, 2018: pp. 23–28. https://doi.org/10.4229/35thEUPVSEC20182018-1AO.2.2.
[15] J. Nishinaga, T. Nagai, T. Sugaya, H. Shibata, S. Niki, Single-crystal Cu(In,Ga)Se2 solar cells grown on GaAs substrates, Appl. Phys. Express. 11 (2018) 082302. https://doi.org/10.7567/APEX.11.082302.
[16] S. Niki, P.J. Fons, A. Yamada, T. Kurafuji, S. Chichibu, H. Nakanishi, W.G. Bi, C.W. Tu, High quality $CuInSe_2$ films grown on pseudo-lattice-matched substrates by molecular beam epitaxy, Appl. Phys. Lett. 69 (1996) 647–649. https://doi.org/10.1063/1.117793.
[17] H. Guthrey, A. Norman, J. Nishinaga, S. Niki, M. Al-Jassim, H. Shibata, Optical and Structural Properties of High-Efficiency Epitaxial $Cu(In,Ga)Se_2$ Grown on GaAs, ACS Appl. Mater. Interfaces. 12 (2020) 3150–3160. https://doi.org/10.1021/acsami.9b18040.
[18] T. Quinci, J. Kuyyalil, T.N. Thanh, Y.P. Wang, S. Almosni, A. Létoublon, T. Rohel, K. Tavernier, N. Chevalier, O. Dehaese, N. Boudet, J.F. Bérar, S. Loualiche, J. Even, N. Bertru, A.L. Corre, O. Durand, C. Cornet, Defects limitation in epitaxial GaP on bistepped Si surface using UHVCVD–MBE growth cluster, Journal of Crystal Growth. 380 (2013) 157–162. https://doi.org/10.1016/j.jcrysgro.2013.05.022.
[19] I. Lucci, S. Charbonnier, M. Vallet, P. Turban, Y. Léger, T. Rohel, N. Bertru, A. Létoublon, J.-B. Rodriguez, L. Cerutti, E. Tournié, A. Ponchet, G. Patriarche, L. Pedesseau, C. Cornet, A Stress-Free and Textured GaP Template on Silicon for Solar Water Splitting, Advanced Functional Materials. 28 (2018) 1801585. https://doi.org/10.1002/adfm.201801585.
[20] C. Cornet, S. Charbonnier, I. Lucci, L. Chen, A. Létoublon, A. Alvarez, K. Tavernier, T. Rohel, R. Bernard, J.-B. Rodriguez, L. Cerutti, E. Tournié, Y. Léger, M. Bahri, G. Patriarche, L. Largeau, A. Ponchet, P. Turban, N. Bertru, Zinc-blende group III-V/group IV epitaxy: Importance of the

miscut, Phys. Rev. Materials. 4 (2020) 053401. https://doi.org/10.1103/PhysRevMaterials.4.053401.
[21] Y. Ping Wang, A. Letoublon, T. Nguyen Thanh, M. Bahri, L. Largeau, G. Patriarche, C. Cornet, N. Bertru, A. Le Corre, O. Durand, Quantitative evaluation of microtwins and antiphase defects in GaP/Si nanolayers for a III–V photonics platform on silicon using a laboratory X-ray diffraction setup, J Appl Cryst. 48 (2015) 702–710. https://doi.org/10.1107/S1600576715009954.
[22] Y. Takagi, H. Yonezu, K. Samonji, T. Tsuji, N. Ohshima, Generation and suppression process of crystalline defects in GaP layers grown on misoriented Si(1 0 0) substrates, Journal of Crystal Growth. 187 (1998) 42–50. https://doi.org/10.1016/S0022-0248(97)00862-2.
[23] Y. Ping Wang, J. Stodolna, M. Bahri, J. Kuyyalil, T. Nguyen Thanh, S. Almosni, R. Bernard, R. Tremblay, M. Da Silva, A. Létoublon, T. Rohel, K. Tavernier, L. Largeau, G. Patriarche, A. Le Corre, A. Ponchet, C. Magen, C. Cornet, O. Durand, Abrupt GaP/Si hetero-interface using bistepped Si buffer, Appl. Phys. Lett. 107 (2015) 191603. https://doi.org/10.1063/1.4935494.
[24] J. Kessler, C. Chityuttakan, J. Lu, J. Schöldström, L. Stolt, Cu(In,Ga)Se2 thin films grown with a Cu-poor/rich/poor sequence: growth model and structural considerations, Progress in Photovoltaics: Research and Applications. 11 (2003) 319–331. https://doi.org/10.1002/pip.495.
[25] A. M. Gabor, J. R. Tuttle, D. S. Albin, M. A. Contreras, R. Noufi, A. M. Hermann, High-efficiency CuInxGa1−xSe2 solar cells made from (Inx,Ga1−x)2Se3 precursor films, Appl. Phys. Lett. 65 (1994) 198–200. https://doi.org/10.1063/1.112670.
[26] J. Kessler, J. Scholdstrom, L. Stolt, Rapid Cu(In,Ga)Se/sub 2/ growth using “end point detection,” in: Conference Record of the Twenty-Eighth IEEE Photovoltaic Specialists Conference - 2000 (Cat. No.00CH37036), 2000: pp. 509–512. https://doi.org/10.1109/PVSC.2000.915883.
[27] J. Kessler, C. Chityuttakan, J. Schöldström, L. Stolt, Growth of Cu(In,Ga)Se2 films using a Cu-poor/rich/poor sequence: substrate temperature effects, Thin Solid Films. 431–432 (2003) 1–5. https://doi.org/10.1016/S0040-6090(03)00222-0.
[28] T. Painchaud, N. Barreau, L. Arzel, J. Kessler, Fast Cu(In,Ga)Se2 precursor growth: Impact on solar cell, Thin Solid Films. 519 (2011) 7221–7223. https://doi.org/10.1016/j.tsf.2011.01.098.
[29] H. Rodriguez-Alvarez, N. Barreau, C.A. Kaufmann, A. Weber, M. Klaus, T. Painchaud, H.-W. Schock, R. Mainz, Recrystallization of Cu(In,Ga)Se2 thin films studied by X-ray diffraction, Acta Materialia. 61 (2013) 4347–4353. https://doi.org/10.1016/j.actamat.2013.04.006.
[30] S. Niki, M. Contreras, I. Repins, M. Powalla, K. Kushiya, S. Ishizuka, K. Matsubara, CIGS absorbers and processes, Progress in Photovoltaics: Research and Applications. 18 (2010) 453–466. https://doi.org/10.1002/pip.969.
[31] A. Chirilă, S. Buecheler, F. Pianezzi, P.Bloesch, C. Gretener, A. R. Uhl, C. Fella, L. Kranz, J. Perrenoud, S. Seyrling, R. Verma, S.Nishiwaki, Y. E. Romanyuk, G. Bilger, A.N. Tiwari, Highly efficient Cu(In,Ga)Se 2 solar cells grown on flexible polymer films, Nature Materials. 10 (2011) 857–861. https://doi.org/10.1038/nmat3122.